J|A|C|S ARTICLES

Published on Web 05/19/2010

From Redox Gating to Quantized Charging

Zhihai Li,[†] Yaqing Liu,[‡] Stijn F. L. Mertens,[†] Ilya V. Pobelov,*[,†] and Thomas Wandlowski*[,†]

Department of Chemistry and Biochemistry, University of Bern, Freiestrasse 3, CH-3012 Bern, Switzerland, and Institute of Bio- and Nanosystems IBN 3 and Center of Nanoelectronic Systems, for Informational Technology, Research Center Jülich, D-52425 Jülich, Germany

Received April 1, 2010; E-mail: thomas.wandlowski@dcb.unibe.ch; ilya.pobelov@iac.unibe.ch

Abstract: Electron transport characteristics were studied in redox molecule-modified tunneling junctions Au(111)|6-thiohexanoylferrocene (Fc6)|solution gap|Au STM tip in the absence and in the presence of gold nanoclusters employing an electrochemical STM setup. We observed transistor- and diode-like current−voltage responses accounted for by the redox process at the ferrocene moiety. We demonstrate that the reorganization energy of the redox site decreases with decreasing gap size. As a unique new feature, we discovered the formation of uniform (size ∼2.4 nm) gold nanoparticles, upon multiple oxidation/reduction cycles of the Fc6 adlayer. The immobilized nanoparticles modify the electron transport response of the Fc6 tunneling junctions dramatically. On top of embedded single nanoparticles we observed single-electron Coulomb charging signatures with up to seven narrow and equally spaced energy states upon electrochemical gating. Our results demonstrate the power of the electrochemical approach in molecular electronics and offer a new perspective toward two-state and multistate electronic switching in condensed media at room temperature.

1. Introduction

Electric transport in nanoscale systems has been the subject of considerable interest during the past few years.[1−4] Substantial efforts have been made to build and to characterize individual molecules that mimic functions of conventional solid-state devices.[5,6] The electric characterization of nanoscopic assemblies (metal|molecule|metal) with devicelike functions, such as rectifiers, switches, or transistors, require source and drain electrodes, preferably an external gate, and one or more low-lying localized molecular electronic levels.[2−4,7,8] A number of experimental approaches have been employed to wire molecules of interest into a molecular junction, such as scanning probe microscopy, crossed wire and nanoparticle junctions, mechanical and electromigration break junctions, nanopores and mercury drop electrodes (see refs 3 and 7−12 and literature cited therein).

Working in an electrochemical environment has the advantage that the electrolyte acts as a unique gate.[3,8,13−16] The field of the electrochemical double layer ($\sim 10^9$ V m^{-1}) is close to the gate field required to significantly modulate the current through a molecular junction according to first-principle calculations by di Ventra et al.[17,18]

Particularly promising systems, although still poorly understood, to construct functional nanojunctions represent redox-active molecules, which are reduced or oxidized by the application of an external voltage.[3,8,19−24] Until now several groups have utilized the concept of "electrolyte gating" and demonstrated with custom-designed molecular hybrid systems amplification and/or rectification in current−voltage characteristics. Examples of redox-active molecular systems employed

[†] University of Bern.
[‡] Research Center Jülich.

(1) Joachim, C.; Ratner, M. A. *Proc. Natl. Acad. Sci. U.S.A.* **2005**, *102*, 8801–8808.
(2) Nitzan, A.; Ratner, M. A. *Science* **2003**, *300*, 1384–1389.
(3) Heath, J. R. *Annu. Rev. Mater. Res.* **2009**, *39*, 1–23.
(4) Cuevas, J. C.; Sheer, E. *Molecular Electronics: An Introduction to Theory and Experiment*; World Scientific: Singapore, 2010.
(5) Carroll, R. L.; Gorman, C. B. *Angew. Chem., Int. Ed.* **2002**, *41*, 4378–4400.
(6) Metzger, R. M. *J. Mater. Chem.* **2008**, *18*, 4364–4396.
(7) Selzer, Y.; Allara, D. L. *Annu. Rev. Phys. Chem.* **2006**, *57*, 593–623.
(8) Chen, F.; Hihath, J.; Huang, Z.; Li, X.; Tao, N. *Annu. Rev. Phys. Chem.* **2007**, *58*, 535–564.
(9) Mantooth, B.; Weiss, P. *Proc. IEEE* **2003**, *91*, 1785–1802.
(10) Kushmerick, J. G.; Blum, A. S.; Long, D. P. *Anal. Chim. Acta* **2006**, *568*, 20–27.
(11) Weiss, E. A.; Kriebel, J. K.; Rampi, M.-A.; Whitesides, G. M. *Philos. Trans. R. Soc. A* **2007**, *365*, 1509–1537.
(12) McCreery, R. L.; Bergren, A. J. *Adv. Mater.* **2009**, *21*, 4303–4322.
(13) White, H. S.; Kittlesen, G. P.; Wrighton, M. S. *J. Am. Chem. Soc.* **1984**, *106*, 5375–5377.
(14) Tao, N. J. *Phys. Rev. Lett.* **1996**, *76*, 4066–4069.
(15) Li, Z.; Han, B.; Meszaros, G.; Pobelov, I.; Wandlowski, T.; Błaszczyk, A.; Mayor, M. *Faraday Discuss.* **2006**, *131*, 121–143.
(16) Rosenblatt, S.; Yaish, Y.; Park, J.; Gore, J.; Sazonova, V.; McEuen, P. L. *Nano Lett.* **2002**, *2*, 869–872.
(17) Ventra, M. D.; Pantelides, S. T.; Lang, N. D. *Appl. Phys. Lett.* **2000**, *76*, 3448–3450.
(18) Ventra, M. D.; Lang, N. D.; Pantelides, S. T. *Chem. Phys.* **2002**, *281*, 189–198.
(19) Lindsay, S. M.; Ratner, M. A. *Adv. Mater.* **2007**, *19*, 23–31.
(20) Zhang, J.; Chi, Q.; Kuznetsov, A. M.; Hansen, A. G.; Wackerbarth, H.; Christensen, H. E. M.; Andersen, J. E. T.; Ulstrup, J. *J. Phys. Chem. B* **2002**, *106*, 1131–1152.
(21) Zhang, J.; Kuznetsov, A. M.; Medvedev, I. G.; Chi, Q.; Albrecht, T.; Jensen, P. S.; Ulstrup, J. *Chem. Rev.* **2008**, *108*, 2737–2791.
(22) Corni, S. *IEEE Trans. Nanotechnol.* **2007**, *6*, 561–570.
(23) Galperin, M.; Ratner, M. A.; Nitzan, A.; Troisi, A. *Science* **2008**, *319*, 1056–1060.
(24) Galperin, M.; Ratner, M. A.; Nitzan, A. *J. Phys. Condens. Mat.* **2007**, *19*, 103201.

are porphyrins,[14,25] viologens,[15,26−30] aniline and thiophene oligomers,[31,32] metal transition complexes,[33−37] carotenes,[38] nitro derivatives of oligophenylene ethynylene,[39,40] ferrocene,[41,42] perylene tetracarboxylic bisimide,[43−45] tetrathiafulvalenes,[30] fullerene derivatives,[46] and redox-active proteins.[20,47−52]

An encouraging approach to construct active molecular circuits involves ferrocene-based systems.[53] The ferrocene/ferrocenium interconversion is fast, and the redox couple is stable in a variety of environments. A wealth of synthetic methods are available to tune the electronic properties of the redox-active ferrocene core and/or to construct a large variety of ferrocene derivatives. Starting from the pioneering work of Chidsey,[54] ferrocene-terminated self-assembled monolayers on gold were developed as model systems for kinetic and thermodynamic studies of Marcus-type electron transfer at electrochemical interfaces.[55−59] The structures of the various adlayers have been characterized by STM,[60−63] infrared, X-ray, and Raman spectroscopy,[57,59,64−66] and quartz crystal microbalance measurements.[57] The unique electrical properties of ferrocene have led to explorative applications in micro- and nanoelectronic hybrid systems. Wrighton et al. reported on the first ferrocene-based molecular device employing the concept of "orthogonal assembly".[67] STM and CP-AFM experiments provided evidence for stochastic switching[42,68] and the occurrence of a negative differential resistance[41,69] in patterned ferrocene-containing self-assembled monolayers. Ex situ electron transport studies at room temperature and under cryogenic conditions employing microfabricated cavities,[70] tunneling junctions of self-assembled monolayers,[71] or a ferrocene-based organometallic wire[72] showed current−voltage characteristics with distinct molecular resonances. Dhirani et al. reported on differential conductance switching in planar tunneling junctions.[73] Explorative studies also suggested novel applications of thin chemisorbed ferrocene films as contact interlayers in photovoltaic cells,[74] electronic memories,[75] or spin valves in spintronics.[76]

(25) Han, W.; Durantini, E. N.; Moore, T. A.; Moore, A. L.; Gust, D.; Rez, P.; Leatherman, G.; Seely, G. R.; Tao, N.; Lindsay, S. *J. Phys. Chem. B* **1997**, *101*, 10719–10725.
(26) Pobelov, I. V.; Li, Z.; Wandlowski, T. *J. Am. Chem. Soc.* **2008**, *130*, 16045–16054.
(27) Haiss, W.; van Zalinge, H.; Higgins, S. J.; Bethell, D.; Höbenreich, H.; Schiffrin, D. J.; Nichols, R. J *J. Am. Chem. Soc.* **2003**, *125*, 15294–15295.
(28) Li, Z.; Pobelov, I.; Han, B.; Wandlowski, T.; Błaszczyk, A.; Mayor, M. *Nanotechnology* **2007**, *18*, 044018.
(29) Haiss, W.; Albrecht, T.; van Zalinge, H.; Higgins, S. J.; Bethell, D.; Höbenreich. ; Schiffrin, D. J.; Nichols, R. J.; Kuznetsov, A. M.; Zhang, J.; Chi, Q.; Ulstrup, J. *J. Phys. Chem. B* **2007**, *111*, 6703–6712.
(30) Leary, E.; Higgins, S. J.; van Zalinge, H.; Haiss, W.; Nichols, R. J.; Nygaard, S.; Jeppesen, J. O.; Ulstrup, J. *J. Am. Chem. Soc.* **2008**, *130*, 12204–12205.
(31) He, H.; Zhu, J.; Tao, N. J.; Nagahara, L. A.; Amlani, I.; Tsui, R. *J. Am. Chem. Soc.* **2001**, *123*, 7730–7731.
(32) Chen, F.; He, J.; Nuckolls, C.; Roberts, T.; Klare, J. E.; Lindsay, S. *Nano Lett.* **2005**, *5*, 503–506.
(33) Albrecht, T.; Guckian, A.; Ulstrup, J.; Vos, J. G. *Nano Lett.* **2005**, *5*, 1451–1455.
(34) Albrecht, T.; Guckian, A.; Kuznetsov, A. M.; Vos, J. G.; Ulstrup, J. *J. Am. Chem. Soc.* **2006**, *128*, 17132–17138.
(35) Albrecht, T.; Moth-Poulsen, K.; Christensen, J. B.; Guckian, A.; Bjørnholm, T.; Vos, J. G.; Ulstrup, J. *Faraday Discuss.* **2006**, *131*, 265–279.
(36) Albrecht, T.; Moth-Poulsen, K.; Christensen, J. B.; Hjelm, J.; Bjørnholm, T.; Ulstrup, J. *J. Am. Chem. Soc.* **2006**, *128*, 6574–6575.
(37) Tran, E.; Duati, M.; Whitesides, G. M.; Rampi, M. A. *Faraday Discuss.* **2006**, *131*, 197–203.
(38) Visoly-Fisher, I.; Daie, K.; Terazono, Y.; Herrero, C.; Fungo, F.; Otero, L.; Durantini, E.; Silber, J. J.; Sereno, L.; Gust, D.; Moore, T. A.; Moore, A. L.; Lindsay, S. M. *Proc. Natl. Acad. Sci. U.S.A.* **2006**, *103*, 8686–8690.
(39) Xiao, X.; Nagahara, L. A.; Rawlett, A. M.; Tao, N. *J. Am. Chem. Soc.* **2005**, *127*, 9235–9240.
(40) He, J.; Fu, Q.; Lindsay, S.; Ciszek, J. W.; Tour, J. M. *J. Am. Chem. Soc.* **2006**, *128*, 14828–14835.
(41) Wassel, R. A.; Credo, G. M.; Fuierer, R. R.; Feldheim, D. L.; Gorman, C. B. *J. Am. Chem. Soc.* **2004**, *126*, 295–300.
(42) Xiao, X.; Brune, D.; He, J.; Lindsay, S.; Gorman, C. B.; Tao, N. *Chem. Phys.* **2006**, *326*, 138–143.
(43) Xu, B.; Xiao, X.; Yang, X.; Zang, L.; Tao, N. *J. Am. Chem. Soc.* **2005**, *127*, 2386–2387.
(44) Li, X.; Hihath, J.; Chen, F.; Masuda, T.; Zang, L.; Tao, N. *J. Am. Chem. Soc.* **2007**, *129*, 11535–11542.
(45) Li, C.; Mishchenko, A.; Li, Z.; Pobelov, I.; Wandlowski, T.; Li, X. Q.; Würthner, F.; Bagrets, A.; Evers, F. *J. Phys.: Condens. Matter* **2008**, *20*, 374122.
(46) Morita, T.; Lindsay, S. *J. Phys. Chem. B* **2008**, *112*, 10563–10572.
(47) Alessandrini, A.; Salerno, M.; Frabboni, S.; Facci, P. *Appl. Phys. Lett.* **2005**, *86*, 133902.
(48) Chi, Q.; Farver, O.; Ulstrup, J. *Proc. Natl. Acad. Sci. U.S.A.* **2005**, *102*, 16203–16208.
(49) Alessandrini, A.; Corni, S.; Facci, P. *Phys. Chem. Chem. Phys.* **2006**, *8*, 4383–4397.
(50) Chi, Q.; Zhang, J.; Jensen, P. S.; Christensen, H. E. M.; Ulstrup, J. *Faraday Discuss.* **2006**, *131*, 181–195.
(51) Liu, Y.; Offenhäusser, A.; Mayer, D. *Biosens. Bioelectron.* **2010**, *25*, 1173–1178.
(52) Davis, J. J.; Peters, B.; Xi, W. *J. Phys.: Condens. Matter* **2008**, *20*, 374123.
(53) Long, N. J. *Metallocenes-An Introduction to Sandwich Complexes*; Blackwell Scientific: Oxford, U.K., 1998.
(54) Chidsey, C. E. D. *Science* **1991**, *251*, 919–922.
(55) Smalley, J. F.; Feldberg, S. W.; Chidsey, C. E. D.; Linford, M. R.; Newton, M. D.; Liu, Y.-P. *J. Phys. Chem.* **1995**, *99*, 13141–13149.
(56) Weber, K.; Hockett, L.; Creager, S. *J. Phys. Chem. B* **1997**, *101*, 8286–8291.
(57) Ye, S.; Haba, T.; Sato, Y.; Shimazu, K.; Uosaki, K. *Phys. Chem. Chem. Phys.* **1999**, *1*, 3653–3659.
(58) Viana, A. S.; Jones, A. H.; Abrantes, L. M.; Kalaji, M. *J. Electroanal. Chem.* **2001**, *500*, 290–298.
(59) Huang, K.; Duclairoir, F.; Pro, T.; Buckley, J.; Marchand, G.; Martinez, E.; Marchon, J.-C.; Salvo, B. D.; Delapierre, G.; Vinet, F. *ChemPhysChem* **2009**, *10*, 963–971.
(60) Viana, A. S.; Abrantes, L. M.; Jin, G.; Floate, S.; Nichols, R. J.; Kalaji, M. *Phys. Chem. Chem. Phys.* **2001**, *3*, 3411–3419.
(61) Müller-Meskamp, L.; Karthäuser, S.; Zandvliet, H. J. W.; Homberger, M.; Simon, U.; Waser, R. *Small* **2009**, *5*, 496–502.
(62) Kruse, P.; Johnson, E. R.; DiLabio, G. A.; Wolkow, R. A. *Nano Lett.* **2002**, *2*, 807–810.
(63) Wedeking, K.; Mu, Z.; Kehr, G.; Fröhlich, R.; Erker, G.; Chi, L.; Fuchs, H. *Langmuir* **2006**, *22*, 3161–3165.
(64) Valincius, G.; Niaura, G.; Kazakevičienė, B.; Talaikytė, Z.; Kažemėkaitė, M.; Butkus, E.; Razumas, V. *Langmuir* **2004**, *20*, 6631–6638.
(65) Watcharinyanon, S.; Moons, E.; Johansson, L. S. O. *J. Phys. Chem. C* **2009**, *113*, 1972–1979.
(66) Shaporenko, A.; Rössler, K.; Lang, H.; Zharnikov, M. *J. Phys. Chem. B* **2006**, *110*, 24621–24628.
(67) Gardner, T. J.; Frisbie, C. D.; Wrighton, M. S. *J. Am. Chem. Soc.* **1995**, *117*, 6927–6933.
(68) Wassel, R. A.; Fuierer, R. R.; Kim, N.; Gorman, C. B. *Nano Lett.* **2003**, *3*, 1617–1620.
(69) Gorman, C. B.; Carroll, R. L.; Fuierer, R. R. *Langmuir* **2001**, *17*, 6923–6930.
(70) Mentovich, E. D.; Kalifa, I.; Tsukernik, A.; Caster, A.; Rosenberg-Shraga, N.; Marom, H.; Gozin, M.; Richter, S. *Small* **2008**, *4*, 55–58.
(71) Nijhuis, C. A.; Reus, W. F.; Whitesides, G. M. *J. Am. Chem. Soc.* **2009**, *131*, 17814–17827.
(72) Getty, S. A.; Engtrakul, C.; Wang, L.; Liu, R.; Ke, S.-H.; Baranger, H. U.; Yang, W.; Fuhrer, M. S.; Sita, L. R. *Phys. Rev. B* **2005**, *71*, 241401.
(73) Dinglasan, J. A. M.; Bailey, M.; Park, J. B.; Dhirani, A. *J. Am. Chem. Soc.* **2004**, *126*, 6491–6497.
(74) Armstrong, N. R.; Carter, C.; Donley, C.; Simmonds, A.; Lee, P.; Brumbach, M.; Kippelen, B.; Domercq, B.; Yoo, S. *Thin Solid Films* **2003**, *445*, 342–352.
(75) Li, Q.; Surthi, S.; Mathur, G.; Gowda, S.; Misra, V.; Sorenson, T. A.; Tenent, R. C.; Kuhr, W. G.; Tamaru, S.; Lindsey, J. S.; Liu, Z.; Bocian, D. F. *Appl. Phys. Lett.* **2003**, *83*, 198–200.

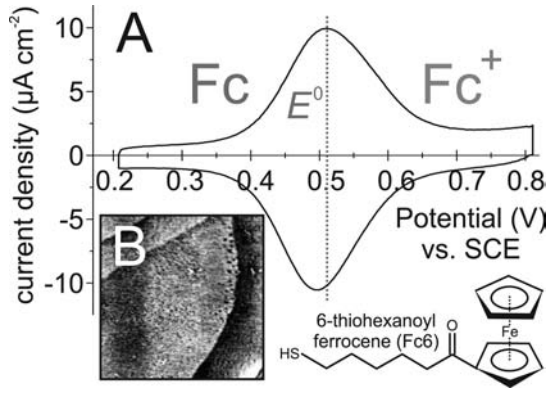

Figure 1. Interfacial properties of a high-coverage monolayer of Fc6 on Au(111)-(1 × 1) in 1.0 M $HClO_4$. (A) Cyclic voltammogram measured with the potential sweep rate $\upsilon = 0.05$ V s^{-1}. The estimated redox potential $E°$ is indicated by the dotted line. (B) In situ STM image. The lateral size is 300 × 300 nm, the vertical scale is 0.6 nm, $I_T = 0.05$ nA, $E_S = 0.1$ V, and $E_T = 0.2$ V.

We report in the present paper on the first construction of a redox-active asymmetric tunneling junction formed between a Au STM tip and a Au(111)-(1 × 1) surface modified with 6-thiohexanoylferrocene (Fc6; Figure 1) in an electrochemical environment. After the description of macroscopic and structure properties of the ferrocene-based monolayer we focus on local in situ tunneling spectroscopy (STS). We demonstrate transistor- and diode-type current−voltage characteristics, both triggered by the local addressing of the redox-active ferrocene moiety. We show that these observations are explained quantitatively by a model assuming a sequential two-step electron transfer with partial vibrational relaxation.[20,21,26] We also illustrate an electrochemical annealing concept, which leads to an unusual transformation of the redox-active tunneling junction into a nanoparticle-mediated junction, which exhibits discrete and locally addressable energy states with unique quantum charging characteristics.[77]

2. Experimental Details

2.1. Electrolytes, Electrodes, and Voltammetric Measurements. The electrolytes were prepared from Milli-Q water (18.2 MΩ, 2 ppb TOC), $HClO_4$ (70%, Merck, suprapure), $LiClO_4$ (Aldrich, 99.99%), and HCl (35%, Merck, suprapure). All electrolytes were deaerated in argon (5 N) before and during the experiments. All measurements were carried out at 22 ± 0.5 °C. The glassware was cleaned in caroic acid followed by extended rinsing with Milli-Q water.

The single-crystal Au(111) electrodes were either cylinders (EC, 4 mm height, 3.6 mm diameter) or disks (STM, 2 mm height and 10 mm diameter). They were flame-annealed with a butane or hydrogen flame at red heat and then cooled slowly in high-purity argon prior to each experiment. Contact with the electrolyte was always established under potential control.

The macroscopic electrochemical measurements were carried out in a three-electrode cell with an Autolab PGSTAT30 (ECO Chemie). A platinum wire and a trapped hydrogen electrode served as counter and reference electrodes. For comparison we converted all potentials given in this paper with reference to a saturated calomel electrode (SCE).

2.2. Electrode Modification. The 6-thiohexanoylferrocene (Fc-$CO(CH_2)_5$-SH, abbreviated Fc6) was synthesized using a previously established procedure[58] and provided by Dr. M. Kalaji, Univerity of Bangor, Bangor, U.K. The modified adlayers were prepared with island-free Au(111)-(1 × 1) electrodes. After flame annealing and lifting of the reconstruction in 0.1 M HCl,[78] these electrodes were immersed in a 1.0 mM ethanolic solution of Fc6 in a sealed argon-filled container for 20 h at room temperature. After incubation, the samples were removed from the solution, carefully rinsed with absolute ethanol, dried under a stream of argon, and subsequently transferred into the electrochemical or STM cell.

2.3. STM and STS Measurements. The electrochemical STM and STS measurements were carried out with a modified Pico-SPM (Agilent) in a sealed, argon-filled chamber. The STM tips were electrochemically etched gold or platinum/iridium (70/30) wires (0.25 mm diameter) coated with polyethylene. Both types of tips are capable of atomic resolution. The leakage current was typically less than 1 pA. Two platinum reference and counter electrodes completed the configuration of the electrochemical cell. This arrangement represents an electrochemical transistor-type assembly with tip and Au(111)-(1 × 1) sample corresponding to source and drain electrodes and the electrolyte as a gate.

Current−voltage curves (I_T vs E) were recorded with gold STM tips in a potential cycle at fixed geometry of the tunneling junction with the feedback being temporarily switched off. In constant bias mode, the bias voltage was fixed, while both E_T and E_S, the potentials of the tip and substrate, were cycled with a rate of 0.5 or 1.0 V s^{-1}. In variable bias mode, E_S was fixed and E_T was cycled in a wide potential range with a rate of 0.5 or 1.0 V s^{-1}. The cycle was repeated 5−10 times for every set of experimental conditions. We note that constant bias mode and variable bias mode correspond to the variation of gate and bias potentials, respectively.

The in situ STS experiments require a high stability of the tip position. The vertical stability was checked by disabling the feedback loop and observing the evolution of the tunneling current with time. The spectroscopic measurements were carried out only if the tip displacement was negligible compared to the recording time of a complete current−voltage trace. Only those scans showing a return of I_T to the initial set point current I_0, after completion of the cycle, were selected for the further analysis. In situ STS and STM measurements were carried out in alternating sequences with the same gold tip to ensure that the experimental system remained intact and reproducible.

3. Results and Discussion

3.1. Adlayer Characterization. A freshly prepared Fc6 monolayer on an Au(111)-(1 × 1) electrode was first characterized by cyclic voltammetry and in situ STM. Figure 1A shows a typical cyclic voltammogram (CV) of the modified gold substrate in 1.0 M $HClO_4$ for a scan rate of $\upsilon = 0.05$ V s^{-1} (see also the Supporting Information, section A). The characteristic pair of peaks represents the reduction and oxidation of the ferrocene moiety.[54] The peak-to-peak separation is close to zero in the measured range of scan rates $0.01 \leq \upsilon \leq 1$ V s^{-1} (Supporting Information, Figure S1A). The peak heights scale linearly with υ (Supporting Information, Figure S1B). These observations point to a reversible redox process within a surface-confined adlayer. The equilibrium potential is estimated to be $E° = 0.51 \pm 0.01$ V. Integration of the oxidation/reduction peaks, assuming a one-electron-transfer reaction, gives the apparent surface coverage $\Gamma = (3.6 \pm 0.4) \times 10^{-10}$ mol cm^{-2}. This value is in agreement with literature data[58,60] and represents a close packing of the Fc6 monolayer with the alkyl spacers almost perpendicular to the surface. The fwhm of the redox

(76) Liu, R.; Ke, S.-H.; Baranger, H. U.; Yang, W. *Nano Lett.* **2005**, *5*, 1959–1962.
(77) Albrecht, T.; Mertens, S. F. L.; Ulstrup, J. *J. Am. Chem. Soc.* **2007**, *129*, 9162–9167.
(78) Hölzle, M. H.; Wandlowski, T.; Kolb, D. M. *J. Electroanal. Chem.* **1995**, *394*, 271–275.

peak amounts to 0.12 ± 0.02 V, indicating repulsive interactions within the adlayer.[79] Immersion experiments[80] with a dry Fc6-modified electrode revealed that the Fc6-covered gold surface bears a positive total charge at $E > 0.35$ V (Supporting Information, section B).

The above data are complemented by high resolution in situ STM images of the Fc6 monolayer on Au(111)-(1 × 1). No long-range order is found (Figure 1B). We observed monoatomically deep vacancies of 2−5 nm in diameter covering the entire surface. This pattern is typical for high-coverage self-assembled monolayers of short-chain thiols on Au(111).[81] Closer inspection reveals that the vacancies are larger nearby upper step edges, while a meander-type pattern is observed next to the lower step edges. The morphology of steps is changing during cycling of the electrode potential in the double-layer region, which indicates rather high dynamics within the redox-active adlayer. We also notice that the double-layer charging current at $E > E°$ is significantly higher as compared to $E < E°$. This observation reflects the coadsorption of ClO_4^- anions with the ferrocenium cation, accompanied by a decrease of the tilt angle of the adlayer upon oxidation.[57,64]

3.2. In Situ Scanning Tunneling Spectroscopy with Redox-Active Tunneling Junctions. Asymmetric tunneling junctions were created between a Fc6-modified Au(111)-(1 × 1) electrode and a gold STM tip. The tip−sample separation was controlled by the bias voltage $E_b = E_S - E_T$, E_S and E_T being the potentials of the Au(111) sample and Au tip, and the preset initial tunneling current I_0. Considering the geometry of the tip as well as the low values of the tunneling conductance I_0/E_b chosen, we ensured that in these experiments junctions with a small number of Fc6 molecules, or even only a single molecule, were sampled. The current−voltage characteristics of the created junctions were measured with the STM feedback disabled. A single measurement started typically with E_S and E_T set in the potential range where the neutral ferrocene moiety is stable. Then E_S and E_T were swept toward values more positive than the equilibrium potential $E°$ and subsequently back to the initial potentials. The stability of the junction geometry was ensured by employing the following protocol. Before each measurement with the STM feedback loop switched off, we monitored the time-dependent evolution of the tunneling current I_T. The spectroscopic measurements were carried out only if current variations due to drift of the tip or other factors were negligible on the time scale of a single current−voltage trace. We used a fast potential sweep rate of 0.5 or 1.0 V s^{-1} to limit the recording time of a complete cycle to less than 2 s. The STM feedback was enabled after every single scan to allow stabilization of the system for a few seconds before the next open-feedback cycle was recorded. For further processing we considered only curves displaying nearly identical forward and backward half-scans and a return of the tunneling current I_T to I_0 at the end of the completed scan. We averaged and analyzed typically 15−20 forward and backward half-cycles per setting, fulfilling the above criteria.

Figure 2 shows typical current−voltage curves measured in constant bias (Figure 2A) and variable bias (Figure 2B) modes. Both types of current−voltage responses were recorded for identical junctions, stabilized at a tunneling conductance I_0/E_b = 1 nS. Figure 2A demonstrates that the tunneling current exhibits a distinct maximum at $E = E_{peak}$, while $I_T \approx I_0$ for $E_{S,T} \ll E^0$ respective $E_{S,T} \gg E°$. In comparison to viologen derivatives,[26] the off-resonance currents at $E_S \leq 0.35$ V and $E_S \geq 0.7$ V are similar, indicating that the potential-induced structure modification of the ferrocene adlayer does not significantly modify the conductance properties of the junctions under nonresonant conditions. No maximum in the tunneling current is observed under the same experimental conditions if the tip is retracted.

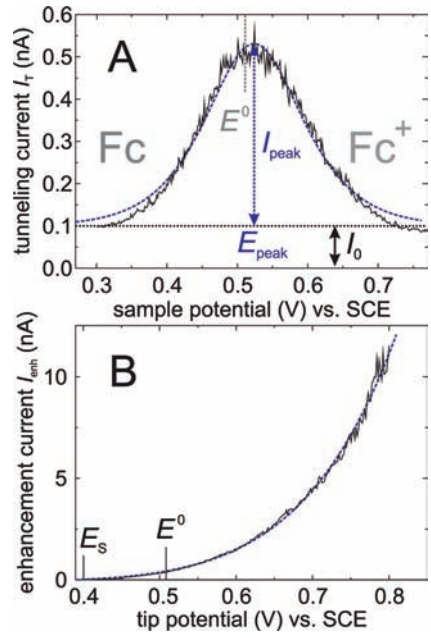

Figure 2. Averaged current−voltage responses of Fc6-based redox-active tunneling junctions obtained from 11 individual traces, at a preset initial tunneling conductance I_0/E_b of 1 nS and with a potential sweep rate of 1 V s^{-1}. Solid black lines are experimental curves, and dashed blue lines are fits of eq 1 to the experimental data. (A) I_T vs E_S characteristics recorded in constant bias mode: $E_b = 0.1$ V, $I_0 = 0.1$ nA. Dotted lines are guides for the eye: (black) $I = I_0$, (gray) $E = E°$, (blue arrow) position $E = E_{peak}$, height I_{peak}. Fitted parameters of eq 1: $\lambda = 0.44$ eV, $\xi = 0.70$, $\gamma = 0.40$. (B) Background-corrected I_{enh} vs E_T characteristics in variable bias mode with $E_S = 0.4$ V and initial $E_T = 0.45$ V; $I_0 = 0.05$ nA. Fitted parameters of eq 1: $\lambda = 0.55$ eV, $\xi = 0.62$, $\gamma = 0.64$.

$$I_{enh} = 1820E_b\left\{\exp\left[\frac{9.73}{\lambda}(\lambda + \xi\eta + \gamma E_b)^2\right] + \exp\left[\frac{9.73}{\lambda}(\lambda + E_b - \xi\eta - \gamma E_b)^2\right]\right\}^{-1} \quad (1)$$

We measured I_T vs E_S characteristics of 93 individual constant bias junctions, initially stabilized at a conductance of 1 nS. The corresponding responses were similar to those plotted in Figure 2A. However, the positions of the current peaks E_{peak} shifted linearly with increasing bias voltage E_b toward lower values (Figure 3A). We note that E_{peak} is close to the equilibrium potential $E°$ of the ferrocene/ferrocenium couple in 0.1 M $HClO_4$ at $E_b = 0$ V.

Figure 2B shows an enhancement of the current I_{enh}, as measured on top of the direct tunneling current (see the Supporting Information, section C) at variable bias potentials upon scanning E_T toward more positive values while keeping E_S fixed. Our results clearly represent a redox-mediated enhancement of the tunneling current. We notice that the overall behavior of a redox-active tunneling junction resembles that of

(79) Bard, A. J.; Faulkner, L. *Electrochemical Methods: Fundamentals and Applications*, 2nd ed.; Wiley: New York, 2001; p 591.
(80) Aguilar-Sanchez, R.; Su, G. J.; Homberger, M.; Simon, U.; Wandlowski, T. *J. Phys. Chem. C* **2007**, *111*, 17409–17419.
(81) Yang, G.; Liu, G. *J. Phys. Chem. B* **2003**, *107*, 8746–8759.

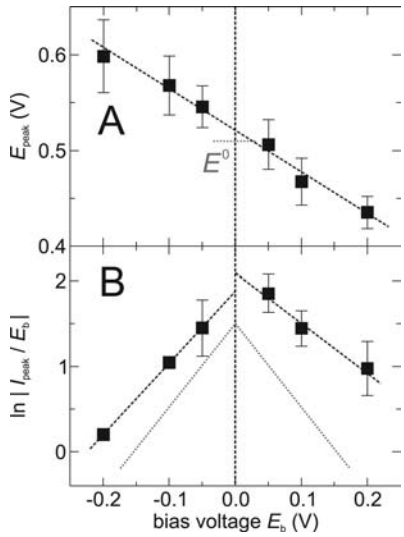

Figure 3. Experimental E_{peak} vs E_b (A) and ln $|I_{peak}/E_b|$ vs E_b (B) dependencies for 93 experimental constant bias current−voltage curves of 1 nS junctions. (A) The dashed blue line represents a linear fit to the experimental data based on eq 2 ($y = (0.52 \pm 0.01) - (0.43 \pm 0.08)E_b$). The dotted line is a guide for the eye corresponding to $E = E°$. (B) The dashed blue lines are linear fits to the experimental data based on eq 3 (positive E_b branch, $y = (2.1 \pm 0.3) - (5.9 \pm 2.6)E_b$; negative E_b branch, $y = (1.9 \pm 0.2) + (8.4 \pm 0.9)E_b$). The dotted lines are guides for the eye with slopes equal to the theoretical values ±9.73.

a conventional solid-state transistor, with sample and probe electrodes being equivalent to source respective drain electrodes and the reference electrode acting as an "electrolyte gate" electrode.

Tunneling characteristics qualitatively similar to those of Fc6 were reported previously for Fe(III) protoporphyrin(IX),[14] metal transition complexes,[33,34] azurine,[49,50] perylene-bisimides,[45] tetrathiafulvalenes,[30] and viologen derivatives[26,28] immobilized in various types of electrochemical nanojunctions. In order to analyze and quantify the observed current enhancement in redox-active Fc6-modified asymmetric tunneling junctions, we consider the following mechanisms: (1) resonance tunneling,[82] (2) vibrationally coherent two-step electron transfer,[83] and (3, 4) noncoherent two-step electron transfer with (3) complete[84] or (4) partial vibrational relaxation.[20,21,26] The first two models predict at small constant bias voltages E_b a maximum of the enhanced tunneling current shifted from the equilibrium redox potential $E°$ approximately by the value of the reorganization energy λ.[20,21] The latter has a typical value of a few hundred millielectronvolts in a tunneling junction[20,21,26,45] and amounts to 0.85 ± 0.10 eV for ferrocene-modified adlayers in a semi-infinite metal−electrolyte configuration.[54−56] The present experimental data cannot account for either one of these models because the position of the enhanced current E_{peak} is too close to the equilibrium potential $E°$ at low bias voltages. The rather high magnitude of the enhanced tunneling current I_{enh} also excludes the third model, which assumes a noncoherent two-step electron transfer with complete vibrational relaxation.

All experimental observations described above support the applicability of the model of a two-step electron transfer with partial vibrational relaxation, developed by Kuznetsov and Ulstrup (KU model).[20,21,26] The model, as represented by the numerical expression (eq 1), predicts characteristic dependencies between the enhanced tunneling current I_{enh}, the bias voltage E_b, and the overpotential $\eta = E_S - E°$.[26] Here I_{enh} is given in nA, E_b and η are given in V, and the reorganization energy λ is given in eV. ξ and γ, both ranging between 0 and 1, are model parameters describing the shift of the effective electrode potential at the reactive center with the variation of η and E_b, respectively. The deduction of eq 1 from the KU model as well as its limitations were extensively described in ref 26. For a more general overview of the topic we refer to a recent review by Ulstrup et al.[21]

Examples of theoretical curves obtained by fitting eq 1 to the experimental current−voltage characteristics in constant and variable bias mode are illustrated by the dashed lines in parts A and B of Figures 2, respectively. The corresponding two sets of model parameters ($\lambda = 0.44$ eV, $\xi = 0.70$, $\gamma = 0.40$ and $\lambda = 0.55$ eV, $\xi = 0.62$, $\gamma = 0.64$) are very similar and lead to an excellent representation of the experimental observations for these two particular sets of data plotted in Figure 2. In an attempt to generalize our conclusions for all current−voltage characteristics recorded for Fc6 in a wide range of bias voltages E_b and overpotentials η, we analyzed the following two correlations quantitatively:

$$E_{peak} = E° + (0.5 - \gamma)E_b/\xi \quad (2)$$

$$\ln |I_{peak}/E_b| = (6.81 - 9.73\lambda) - 9.73|E_b| \quad (3)$$

These expressions describe the dependencies of position and height of the peak of the enhanced tunneling current in constant bias mode, E_{peak} and I_{peak} (Figure 2A), on the bias voltage E_b. They were derived on the basis of the KU model and eq 1.[21,26] Figure 3 shows plots of E_{peak} vs E_b (eq 2) and ln $|I_{peak}/E_b|$ vs E_b (eq 3). These graphs represent E_{peak} and I_{peak} values, extracted from 93 individual constant bias current−voltage characteristics. The junction conductance prior to the voltage sweep was always fixed to 1 nS in the stability region of the neutral ferrocene moiety, ensuring a constant separation between STM tip and Fc6-modified gold substrate. The linear variations of the average values of E_{peak} (Figure 3A) and ln $|I_{peak}/E_b|$ (Figure 3B) upon changing E_b are in excellent agreement with eqs 2 and 3. We notice that the plot of ln $|I_{peak}/E_b|$ vs E_b shows two linear branches, which approach each other at $E_b \rightarrow 0$. The slopes of both branches are close to the theoretical values (dotted lines in Figure 3B). The intercepts lead to the following values of the reorganization energy:, $\lambda = 0.48 \pm 0.03$ eV for the positive branch and $\lambda = 0.51 \pm 0.02$ eV for the negative branch. Linear fits of the ln $|I_{peak}/E_b|$ vs E_b dependencies with a fixed slope (not shown) resulted in the estimations $\lambda = 0.45 \pm 0.01$ eV (positive branch) and $\lambda = 0.48 \pm 0.01$ eV (negative branch). We emphasize that these values of λ agree with the parameters obtained from individual fits of eq 1 to experimental curves such as those plotted in Figure 2.

We also studied the dependence of the junction properties on tip−sample separation. The latter was controlled by the variation of the initial set point current (0.05 nA $\leq I_0 \leq 10$ nA) at fixed $E_b = 0.1$ V. Although the absolute probe−electrode separation has not been determined in our STM configuration, we may state that an increase of the off-resonance tunneling conductance I_0/E_b corresponds to a reduction of the tip−sample distance. We measured a series of 10 constant bias current−voltage curves for each I_0 value and determined the average value of I_{peak} (cf. Figure 2A). The latter is monotonously increasing with

(82) Schmickler, W.; Tao, N. *Electrochim. Acta* **1997**, *42*, 2809–2815.
(83) Kuznetsov, A.; Ulstrup, J. *Electrochim. Acta* **2000**, *45*, 2339–2361.
(84) Kuznetsov, A. M.; Ulstrup, *J. Chem. Phys.* **1991**, *157*, 25–33.

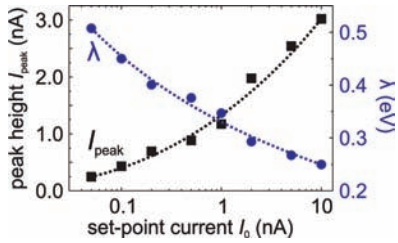

Figure 4. Dependence of I_{peak} (black squares, scale on the left) and the corresponding value of the reorganization energy λ (blue circles, scale on the right) on the initial set-point current I_0 at fixed value of $E_b = 0.1$ V. Each data point corresponds to the average of 10 experimental curves. The dotted lines are guides for the eye.

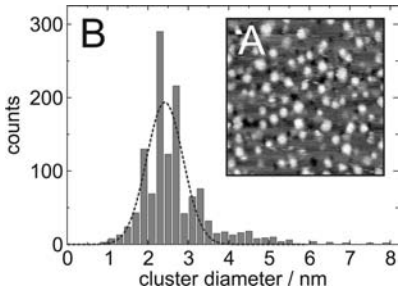

Figure 5. (A) STM image of gold clusters formed within the Fc6 adlayer by multiple potential cycles in the tunneling regime in 0.2 V $\leq E_{S,T} \leq$ 0.80 V. The lateral size is 50 × 50 nm, the vertical scale is 0.4 nm, $I_T = 0.05$ nA, $E_S = 0.7$ V, and $E_T = 0.1$ V. (B) Size distribution histogram of 1264 clusters from 15 STM images and its Gaussian fit. The corresponding parameters are the average cluster diameter 2.42 nm and the standard deviation $\sigma = 0.45$ nm.

I_0 (Figure 4). The corresponding reorganization energies λ were subsequently calculated with eq 3 using the experimentally accessible values of I_{peak} and E_b. We found that λ decreases with an increase of I_0 (Figure 4). Specifically, the λ values of the Fc6-modified tunneling junctions decrease from ~0.5 eV to ~0.25 eV upon a 200-fold increase of I_0. The maximum value is significantly smaller as compared to 0.85 ± 0.10 eV, which is found for ferrocene-modified adlayers in a semi-infinite metal−electrolyte configuration.[54−56] The decrease of the reorganization energy λ upon closure of the tunneling gap, as experimentally observed for the first time in the present study, may be rationalized physically by a reduction of the solvent space surrounding the redox center.[85]

3.3. Transformation of the Fc6 Adlayer. After multiple cycles of Fc6 oxidation and reduction during the STS measurements in the potential range 0.20 $\leq E_{S,T} \leq$ 0.80 V, we monitored the stability and redox activity of the Fc6 adlayer up to 20 h. We found that the macroscopic CV response (Figure 1A) did not change if the whole system is carefully protected from oxygen under an inert Ar atmosphere. However, the morphology of the surface, as imaged by in situ STM, showed a distinct modification (Figure 5A). We observed the formation of small gold clusters within the redox-active ferrocene-terminated adlayer. The clusters are rather immobile and appear to be trapped within the organic layer. The size distribution of the clusters is rather narrow (Figure 5B). We estimate an average diameter of 2.4 ± 0.5 nm. The origin of these clusters is attributed to the partial decomposition of the ferrocene-based adlayer[57] accompanied by the local release of gold surface atoms and their subsequent aggregation.[86]

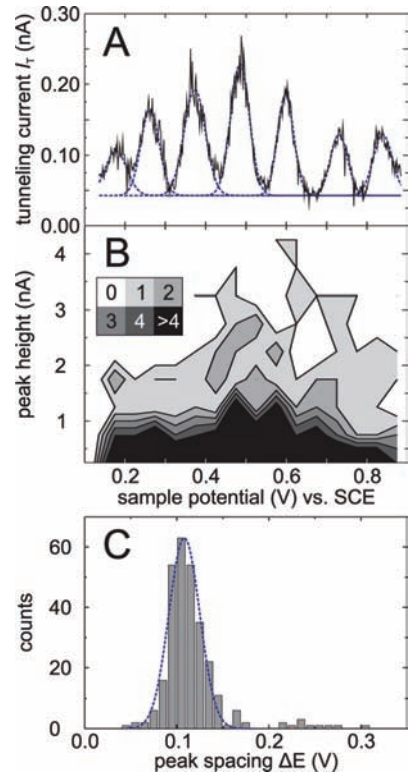

Figure 6. (A) Example of a constant bias current−voltage response I_T vs E_S of a single cluster, $E_b = 0.1$ V, $I_0 = 0.05$ nA, and its fit by a series of Gaussians. (B) Contour map of peak position−peak height distribution for 361 peaks. The various shadings indicate areas with different amounts of counts per cell (0.05 V × 0.5 nA) inside. (C) Peak spacing histogram for the same data set as in (B) and its Gaussian fit. The corresponding parameters are the average spacing 0.11 V and $\sigma = 0.017$ V.

The small size of these immobilized gold nanoparticles suggests that they may possess specific, locally addressable electronic properties.[77,87−89] Thus, we carried out a series of systematic constant bias mode in situ STS experiments with the gold tip positioned above a single gold cluster. Instead of one broad peak as recorded for the bare Fc6 monolayer (Figure 2A), we observed for the cluster-modified junctions up to seven clearly resolved narrow peaks in the $I_T - E_S$ characteristics (Figure 6A). These data were analyzed by fitting a series of Gaussians to deconvolute individual peaks and to determine their positions, heights, and widths. An example is presented in Figure 6A. The peak-to-peak spacing in the current−voltage curves, based on a statistical analysis of 73 individual traces, was found to be very regular (Figure 6C) and equal to 0.11 ± 0.02 V. The full width at half-maximum (fwhm) is also rather uniform and amounts to 0.07 ± 0.03 V. On the other hand, we observed that the measured heights of the individual peaks vary by 2 orders of magnitude and are distributed exponentially with a decay factor of ~0.5 nA (see the Supporting Information, section D). We also noticed that the peaks positioned next to $E \approx E^\circ = 0.51$ V are typically higher than those at more negative or positive potentials, respectively. In an attempt to generalize this observation, we constructed two-dimensional peak position−peak height distributions based on all experimental data accessible.

(85) Corni, S. *J. Phys. Chem. C* **2005**, *109*, 3423–3430.
(86) Taylor, R.; Torr, N.; Huang, Z.; Li, F.; Guo, Q. *Surf. Sci.* **2010**, *604*, 165–170.
(87) Murray, R. W. *Chem. Rev.* **2008**, *108*, 2688–2720.
(88) Zabet-Khosousi, A.; Dhirani, A. *Chem. Rev.* **2008**, *108*, 4072–4124.
(89) Laaksonen, T.; Ruiz, V.; Liljeroth, P.; Quinn, B. M. *Chem. Soc. Rev.* **2008**, *37*, 1836–1846.

The plot in Figure 6B clearly supports the trend formulated. On the basis of the distribution of peak spacings and peak heights we attribute our observations to a modulation of the tunneling current enhancement in the redox-active tunneling junction by a sequential capacitive charging of single gold nanoclusters. Following this hypothesis, we estimate[87,89−91] the average single-particle capacitance $C = e/\Delta E = 1.5 \pm 0.2$ aF. Similar values of C were reported by Chen et al.[92] on the basis of macroscopic voltammetric experiments with a monolayer of alkanethiol-protected nanoparticles immobilized on a gold substrate. Single-electron Coulomb charging was observed for different types and sizes of individual nanoparticles on bare and adsorbate-covered nanoparticles using different approaches. These include specifically STM and STS under vacuum[93−96] or in air.[96,97] Recently, Albrecht et al. published the first STS data in an electrochemical environment.[77] These authors immobilized an alkanethiol-capped Au_{147} nanoparticle in a tunneling junction composed of a Pt/Ir STM tip and a cluster-modified Pt(111) substrate. We note that this nanoscale system did not contain redox-active molecules and that the observed modulation of the tunneling current was asymmetric, which is different from the present work. On the other hand, our study and the work of Albrecht et al. report as a unique result peak-shaped modulations of the tunneling current. The peaks are equally spaced as well as rather close and narrow, which offer new perspectives on multistate electronic switching in condensed media at room temperature. The observed feature of sequential capacitive charging is reminiscent of a successive electronic charging of redox molecules through several oxidation/reduction states. However, the latter are usually much wider than the former. We note that the present system has one accessible molecular redox state in the tunneling junction. The interplay of this redox resonance with the sequential charging of the gold nanoparticles in an individual electrochemical tunneling junction has not yet been treated theoretically, although the Coulomb charging effect under electrochemical conditions in a multistate redox molecule was recently addressed and the results seem to be in agreement with our observations.[98] However, we believe that an appropriate model will need to consider the successive charging of the particle Coulomb levels in combination with the solvent activation and relaxation as modified by the redox-active host lattice.[98−100]

4. Conclusions

We have employed an electrochemical STM approach to demonstrate electrolyte gating, rectification, and quantum charging in a redox-active molecular tunneling junction. The latter is constructed from 6-thiohexanoylferrocene (Fc6) molecules immobilized on an Au(111)-(1 × 1) electrode in the absence as well as in the presence of Au nanoparticles.

The Au substrate|Fc6|solution gap|Au STM tip junctions exhibit an enhanced tunneling current upon alignment of tip and substrate Fermi levels with the molecular redox state. Depending on the applied polarization mode, transistor- or diode-like responses were demonstrated. These gating/rectification effects are accounted for by the dynamics of the solvent reorganization upon charging/discharging the redox center in the tunneling junction. They are quantitatively described by the Kuznetsov−Ulstrup model of a two-step electron transfer with partial vibrational relaxation. For the first time we demonstrate experimentally that the solvent reorganization energy upon oxidation/reduction of the redox moiety decreases with decreasing gap size. This observation is attributed to the reduction of the solvent space surrounding the active center.

Multiple cycles of adlayer oxidation/reduction lead to the formation of Au nanoclusters immobilized within the Fc6 monolayer. The clusters exhibit a narrow size distribution with an average diameter of 2.4 nm. Local STS experiments with these Au(111)|Fc6 + Au nanoparticles|solution gap|Au tip junctions revealed a series of narrow, equally spaced current peaks. We demonstrate that this unique current−voltage response can be attributed to a distinct modulation of the tunneling current by the quantized single-electron charging of the Au nanoparticles. This first study of electronic properties of a tunneling junction composed of redox-active molecules and nanoparticles opens new experimental and theoretical perspectives toward multistate electronic switching in condensed media at room temperature.

In a broader perspective, we aimed to demonstrate that the electrochemical approach offers a unique ability to tune potentials (Fermi levels) of probing electrodes as well as a wide range of functionalized nanoassemblies confined in the gap, and this opens opportunities to control electron transport at a molecular respective single-cluster level, leading toward exciting new phenomena and applications in "wet electronics".

Acknowledgment. This work was supported by the Swiss National Science Foundation (200021_124643; NFP 62), the Volkswagen Foundation, FUNMOLS, and the DFG priority program 1243. S.F.L.M. acknowledges the receipt of an MC fellowship. We also acknowledge Dr. M. Kalaji, Univerity of Bangor, Bangor, U.K., for the generous gift of the Fc6 sample.

Supporting Information Available: Figures and text giving details of cyclic voltammetry and immersion experiments carried out with Fc6 monolayers, background correction of the curve shown in Figure 2B, and a histogram of the peak height distribution for the data presented in Figure 6B,C. This material is available free of charge via the Internet at http://pubs.acs.org.

JA102754N

(90) Chen, S.; Murray, R. W.; Feldberg, S. W. *J. Phys. Chem. B* **1998**, *102*, 9898–9907.
(91) Chen, S.; Murray, R. W. *J. Phys. Chem. B* **1999**, *103*, 9996–10000.
(92) Chen, S.; Pei, R. *J. Am. Chem. Soc.* **2001**, *123*, 10607–10615.
(93) Dubois, J.; Gerritsen, J.; Schmid, G.; van Kempen, H. *Physica B* **1996**, *218*, 262–264.
(94) Andres, R. P.; Bein, T.; Dorogi, M.; Feng, S.; Henderson, J. I.; Kubiak, C. P.; Mahoney, W.; Osifchin, R. G.; Reifenberger, R. *Science* **1996**, *272*, 1323–1325.
(95) Ingram, R. S.; Hostetler, M. J.; Murray, R. W.; Schaaff, T. G.; Khoury, J. T.; Whetten, R. L.; Bigioni, T. P.; Guthrie, D. K.; First, P. N. *J. Am. Chem. Soc.* **1997**, *119*, 9279–9280.
(96) Speets, E. A.; Dordi, B.; Ravoo, B. J.; Oncel, N.; Hallbäck, A.-S.; Zandvliet, H. J. W.; Poelsema, B.; Rijnders, G.; Blank, D. H. A.; Reinhoudt, D. N. *Small* **2005**, *1*, 395–398.
(97) Nijhuis, C. A.; Oncel, N.; Huskens, J.; Zandvliet, H. J. W.; Ravoo, B. J.; Poelsema, B.; Reinhoudt, D. N. *Small* **2006**, *2*, 1422–1426.
(98) Kuznetsov, A. M.; Medvedev, I. G.; Ulstrup, J. *J. Chem. Phys.* **2009**, *130*, 164703.
(99) Mertens, S. F. L.; Blech, K.; Sologubenko, A. S.; Mayer, J.; Simon, U.; Wandlowski, T. *Electrochim. Acta* **2009**, *54*, 5006–5010.
(100) Mertens, S. F. L.; Meszaros, G.; Wandlowski, T. *Phys. Chem. Chem. Phys.* **2010**, *12*, 5417−5424.